

Interplay between field-induced and frustration-induced quantum criticalities in the frustrated two-leg Heisenberg ladder

Brandon W. Ramakko and Mohamed Azzouz*

*Laurentian University, Department of Physics,
Ramsey Lake Road, Sudbury, Ontario P3E 2C6, Canada.*

(Dated: August 21, 2007)

The antiferromagnetic Heisenberg two-leg ladder in the presence of frustration and an external magnetic field is a system that is characterized by two sorts of quantum criticalities, not only one. One criticality is the consequence of intrinsic frustration, and the other one is a result of the external magnetic field. So the behaviour of each of them in the presence of the other deserves to be studied. Using the Jordan-Wigner transformation in dimensions higher than one and bond-mean-field theory we examine the interplay between the field-induced and frustration-induced quantum criticalities in this system. The present work could constitute a prototype for those systems showing multiple, perhaps sometimes competing, quantum criticalities. We calculate several physical quantities like the magnetization and spin susceptibility as functions of field and temperature.

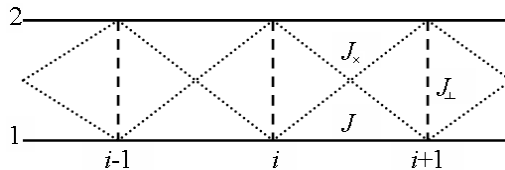


FIG. 1: The two-leg ladder showing the couplings along the chains, rungs, and diagonals is displayed.

I. INTRODUCTION

In low-dimensional antiferromagnetic (AF) Heisenberg spin ladders, the mixing of magnetic frustration, external magnetic fields, and thermal fluctuations together with quantum fluctuations is a recipe for interesting non-conventional and exotic behaviours. The two-leg frustrated ladder is an example, which is characterized by three distinct non-magnetic quantum spin liquid states; the Néel-type (N-type) state, ferromagnetic-type rung (R-type) state, and ferromagnetic-type chain (F-type) state. These states are characterized by ferromagnetic spin arrangements along the diagonals, rungs, or chains respectively. In a recent work, we studied the effect of thermal fluctuations on these states and found that the quantum phase transitions between the R-type and N-type states on one hand and between the R-type and F-type states on the other hand evolve with temperature into classical phase transitions between these disordered states¹. Numerical studies^{2,3} have shown that in the presence of a magnetic field, frustration is able to stabilize a magnetization plateau at half the saturation magnetization. In terms of the Jordan-Wigner (JW) fermions⁴, this would mean that a plateau in the magnetization appears because of the appearance of an energy gap between two (excitation) energy bands. In this paper we will check this claim within the analytical bond-mean-field theory (BMFT)^{1,4,5,6,7}. We will discuss the interplay between the quantum criticality induced by frustration and that produced by magnetic field. Indeed, magnetic field has been shown recently to induce quantum criticality between two distinct states, one characterized by spin bond “order” and the other one by no spin bond order, in the Heisenberg chain and non-frustrated two-leg ladder⁷. Note that spin bond order does not imply any kind of magnetic long range order; i.e., all the states are magnetically disordered in agreement with the Mermin-Wagner theorem⁸.

In section II the BMFT is briefly reviewed. In section III the magnetization, phase diagram, mean-field parameters, energy spectra, and susceptibility are examined. In section IV conclusions are drawn.

II. METHOD

We apply BMFT following the method described in Ref.⁷. The Hamiltonian for the spin- $\frac{1}{2}$ two-leg ladder with diagonal interactions in a magnetic field is written as

$$H = J \sum_i \sum_{j=1}^2 \mathbf{S}_{i,j} \cdot \mathbf{S}_{i+1,j} + J_{\perp} \sum_i \mathbf{S}_{i,1} \cdot \mathbf{S}_{i,2} + J_{\times} \sum_i (\mathbf{S}_{i,1} \cdot \mathbf{S}_{i+1,2} + \mathbf{S}_{i+1,1} \cdot \mathbf{S}_{i,2}) - h \sum_i \sum_{j=1}^2 S_{i,j}^z, \quad (1)$$

where J is the coupling along the chains, J_{\perp} the transverse coupling, and J_{\times} the coupling along the diagonals as seen in Fig. 1. The index i labels the position of the spins along the two chains, each of which has N sites. The first term represents the interactions of nearest-neighboring spins along the chains (legs) of the ladder, the second term represents the interactions of the spins along the rungs, and the third term sums the interactions along the diagonals. As usual, $\mathbf{S}_{i,j}$ is the spin operator. Here $h = g\mu_B B$ with B being the magnetic field, g the Landé factor, and μ_B the Bohr magneton.

The JW transformation^{4,9} for the two-leg Heisenberg ladder is defined as⁶

$$\begin{aligned} S_{i,j}^- &= c_{i,j} e^{i\phi_{i,j}}, & S_{i,j}^z &= n_{i,j} - 1/2, & n_{i,j} &= c_{i,j}^\dagger c_{i,j}, \\ \phi_{i,1} &= \pi \left[\sum_{d=0}^{i-1} \sum_{f=1}^2 n_{d,f} \right], & \phi_{i,2} &= \pi \left[\sum_{d=0}^{i-1} \sum_{f=1}^2 n_{d,f} + n_{i,1} \right]. \end{aligned} \quad (2)$$

Here i and j are the coordinates along the chain and rung directions, respectively. The phases $\phi_{i,j}$ are chosen so that all the spin commutation relations are preserved. The $c_{i,j}^\dagger$ operator creates a spinless fermion at site (i,j) , while $c_{i,j}$ annihilates one, and $n_{i,j}$ is the occupation number operator. Using (2), the Hamiltonian (1) becomes

$$\begin{aligned} H &= \frac{J}{2} \sum_i (c_{i,1}^\dagger e^{i\pi n_{i,2}} c_{i+1,1} + c_{i,2}^\dagger e^{i\pi n_{i+1,1}} c_{i+1,2} + \text{H.c.}) + \frac{J_\perp}{2} \sum_i (c_{i,1}^\dagger c_{i,2} + \text{H.c.}) \\ &+ \frac{J_\times}{2} \sum_i (c_{i,1}^\dagger e^{i\pi(n_{i,2}+n_{i+1,1})} c_{i+1,2} + c_{i+1,1}^\dagger c_{i,2} + \text{H.c.}) + J \sum_i \sum_{j=1}^2 (n_{i,j} - \frac{1}{2})(n_{i+1,j} - \frac{1}{2}) \\ &+ J_\perp \sum_i (n_{i,1} - \frac{1}{2})(n_{i,2} - \frac{1}{2}) + J_\times \sum_i [(n_{i,1} - \frac{1}{2})(n_{i+1,2} - \frac{1}{2}) \\ &+ (n_{i+1,1} - \frac{1}{2})(n_{i,2} - \frac{1}{2})] - h \sum_i \sum_{j=1}^2 (n_{i,j} - \frac{1}{2}). \end{aligned} \quad (3)$$

After applying the JW transformation the Ising terms are decoupled using the Hartree-Fock approximation, which neglects fluctuations around the mean field points; $(O - \langle O \rangle)(O' - \langle O' \rangle) \approx 0$, where O and O' are quadratic in c^\dagger and c ⁵. To apply BMFT we introduce three mean-field bond parameters; Q in the longitudinal direction, P in the transverse direction, and P' along the diagonal. These can be interpreted as effective hopping energies for the JW fermions in the longitudinal, transverse and diagonal directions, respectively⁴:

$$Q = \langle c_{i,j} c_{i+1,j}^\dagger \rangle, \quad P = \langle c_{i,j} c_{i,j+1}^\dagger \rangle, \quad P' = \langle c_{i+1,j} c_{i,j+1}^\dagger \rangle. \quad (4)$$

We choose to place an alternating phase of π along the chains so that the phase per plaquette is π^{10} . This configuration is used to get rid of the phase terms in the Hamiltonian. We also set $Q_{i,j} = Q e^{i\Phi_{i,j}}$ where Q is site independent⁷. Here $\Phi_{i,j}$ is the phase of the bond along the chain such that $\phi = \pi$ or 0 . This is necessary in order to recover the proper result in the limit J_\times and J_\perp becoming zero, in which we get a result comparable to that of des Cloiseaux and Pearson¹¹ for the spin excitation spectrum for a single Heisenberg chain, $E(k) = \frac{\pi}{2} J |\sin k|$.

The magnetization per site is $M_z = \langle S_{i,j}^z \rangle = \langle n_{i,j} \rangle - \frac{1}{2}$. Once a magnetic field is applied the magnetization must be included in the decoupling of the Ising terms. The latter must be decoupled as many ways as is physically acceptable in order to account for all effects. So in addition to the previous two ways¹ it is now decoupled in the following third way:

$$J S_{i,j}^z S_{i+1,j}^z \approx J M_z c_{i+1,j}^\dagger c_{i+1,j} + J c_{i,j}^\dagger c_{i,j} M_z - J M_z^2 - J M_z. \quad (5)$$

The mean-field Hamiltonian becomes

$$H = \sum_k \Psi_k^\dagger \mathcal{H} \Psi_k + 2N Q^2 + N J_\perp P^2 + N h - N(2J + 2J_\times + J_\perp) M_z (M_z + 1). \quad (6)$$

As mentioned in the introduction, when $J_\times \ll J_\perp$, the system adopts the N-type state with ferromagnetic spin arrangements along the diagonals. When $J_\times \gg J_\perp$ the system adopts the R-type state. In this case, the AF spin arrangements shift to the diagonals, and spins on the rungs are forced to adopt a ferromagnetic arrangement. When $J_\times \gg J$ and $J_\perp \gg J$, the system adopts the F-type state, where the spins on the chains adopt a

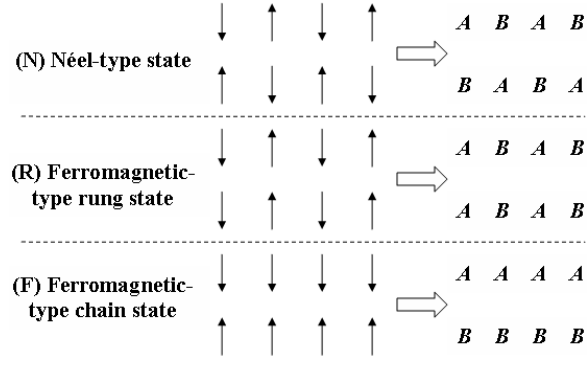


FIG. 2: In the left panel, the three possible ground states of the system in the Ising limit are drawn. In the right panel, the labeling of sublattices corresponding to the short-range spin orders that replace the long-range ones in the Heisenberg limit are shown.

ferromagnetic arrangement and an AF one on the rungs. We use the spin arrangements on the right panel in Fig. 2, where the lattice is subdivided into two sublattices, as a starting point. The Hamiltonian density for the N-type state is given by

$$\mathcal{H} = \begin{pmatrix} -h' & iJ_1 \sin k & J_{\times 1} \cos k & \frac{J_{\perp 1}}{2} \\ -iJ_1 \sin k & -h' & \frac{J_{\perp 1}}{2} & J_{\times 1} \cos k \\ J_{\times 1} \cos k & \frac{J_{\perp 1}}{2} & -h' & iJ_1 \sin k \\ \frac{J_{\perp 1}}{2} & J_{\times 1} \cos k & -iJ_1 \sin k & -h' \end{pmatrix}, \quad (7)$$

where

$$\begin{aligned} J_1 &= J(1 + 2Q), \\ J_{\perp 1} &= J_{\perp}(1 + 2P), \\ J_{\times 1} &= J_{\times}(1 + 2P'), \\ h' &= h - (2J + 2J_{\times} + J_{\perp})M_z. \end{aligned} \quad (8)$$

Diagonalizing \mathcal{H} yields the following four eigenenergies

$$\begin{aligned} E_{N1}(k) &= -h' + J_{\times 1} \cos k + \sqrt{J_1^2 \sin^2 k + \frac{J_{\perp 1}^2}{4}}, \\ E_{N2}(k) &= -h' - J_{\times 1} \cos k + \sqrt{J_1^2 \sin^2 k + \frac{J_{\perp 1}^2}{4}}, \\ E_{N3}(k) &= -h' + J_{\times 1} \cos k - \sqrt{J_1^2 \sin^2 k + \frac{J_{\perp 1}^2}{4}}, \\ E_{N4}(k) &= -h' - J_{\times 1} \cos k - \sqrt{J_1^2 \sin^2 k + \frac{J_{\perp 1}^2}{4}}. \end{aligned} \quad (9)$$

Similarly, the eigenenergies for the F-type state and for the R-type state are given respectively by

$$\begin{aligned} E_F(k) &= -h' \pm J_1 \cos k \pm \sqrt{J_{\times 1}^2 \sin^2 k + \frac{J_{\perp 1}^2}{4}}, \\ E_R(k) &= -h' \pm \frac{J_{\perp 1}}{2} \pm \sqrt{J_1^2 \sin^2 k + J_{\times 1}^2 \cos^2 k}. \end{aligned} \quad (10)$$

The free energy per site is

$$F = JQ^2 + \frac{J_{\perp}P^2}{2} + J_{\times}P'^2 + \frac{h}{2} - (J + J_{\times} + \frac{J_{\perp}}{2})M_z(M_z + 1) - \frac{k_B T}{4N} \sum_k \sum_{p=1}^4 \ln[1 + e^{-\beta E_{\kappa p}(k)}], \quad (11)$$

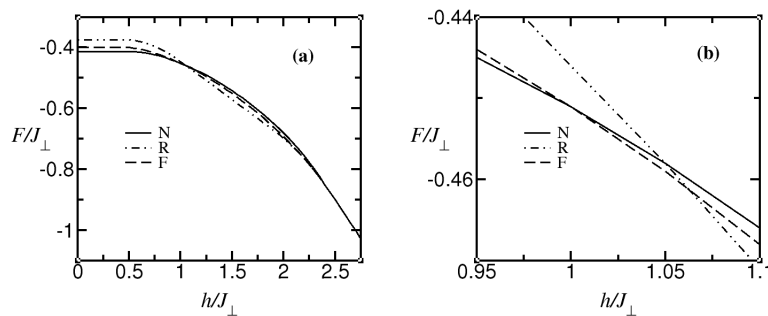


FIG. 3: (a) The free energies are plotted as functions of magnetic field for $J = 0.5J_{\perp}$, and $J_{\times} = 0.4J_{\perp}$. (b) The field-induced transitions are shown by zooming in on fields near the critical fields.

where $\kappa \equiv N, R$, or F depending on the state considered. $E_{\kappa p}(k)$ designates one of the four eigenenergies in state κ . The magnetization can be calculated using $M_z = -\frac{\partial F}{\partial h}$, which gives

$$M_z = -\frac{1}{2} + \frac{1}{4N} \sum_k \sum_{p=1}^4 n_F[E_{\kappa p}(k)]. \quad (12)$$

This adds another equation to the set of self-consistent equation satisfied by the spin bond parameters Q , P , and P' , which are obtained by minimizing the free energy:

$$\begin{aligned} Q &= -\frac{1}{8NJ} \sum_k \sum_{p=1}^4 \frac{\partial E_{\kappa p}(k)}{\partial Q} n_F[E_{\kappa p}(k)], \\ P &= -\frac{1}{4NJ_{\perp}} \sum_k \sum_{p=1}^4 \frac{\partial E_{\kappa p}(k)}{\partial P} n_F[E_{\kappa p}(k)], \\ P' &= -\frac{1}{8NJ_{\times}} \sum_k \sum_{p=1}^4 \frac{\partial E_{\kappa p}(k)}{\partial P'} n_F[E_{\kappa p}(k)]. \end{aligned} \quad (13)$$

The equations in (13) are solved numerically in order to obtain the free energies, magnetization, bond parameters, and uniform spin susceptibility as functions of magnetic field and temperature.

III. RESULTS

A. Free energies

The free energies are compared as seen in Fig. 3 to determine the state with the lowest free energy, which is in turn used to obtain the parameters and magnetization. As Fig 3b shows for the given coupling constants set, a first transition occurs from the N-type state to the F-type state, then another one from the F-type state to the R-type state. Note that this couple of transitions was not mentioned in Ref.², which used the Lanczos method. Our approach works well for analyzing the effect of magnetic field when $J_{\times} = 0$ ⁷, and when $h = 0$ and $J_{\times} \neq 0$ ¹. Including both J_{\times} and h may be pushing the the current mean-field approach to its limits. In the strong field regime all free energies are equal because the magnetization has saturated and all AF fluctuations have disappeared; i.e., even short-range AF correlations are absent in the saturated ferromagnetic state.

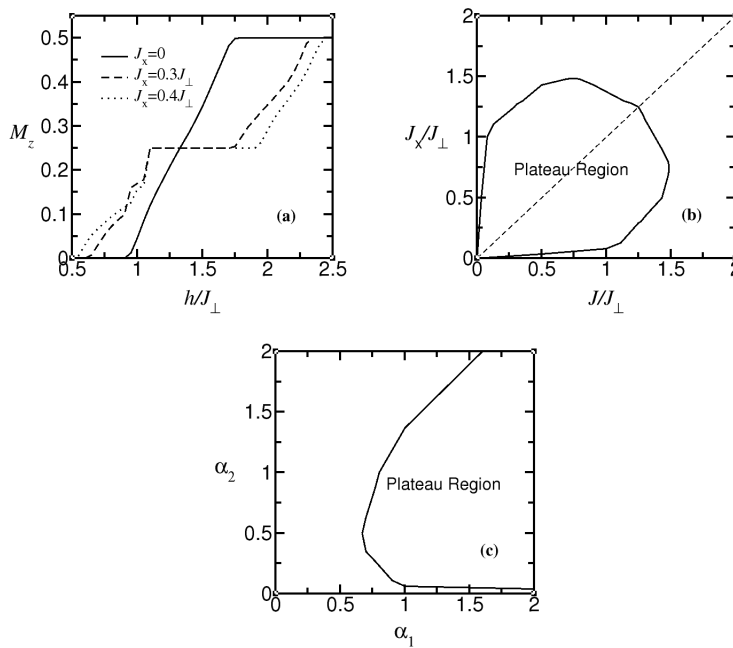


FIG. 4: (a) The magnetization is plotted as a function of h/J_\perp for $J = 0.5J_\perp$ and for the values of J_\times/J_\perp given in the legend. The $(J/J_\perp, J_\times/J_\perp)$ and $(\alpha_1 = J_\perp/J, \alpha_2 = J_\times/J)$ phase diagrams at $M_z = 0.25$ are displayed in (b) and (c), respectively.

B. Magnetization and phase diagrams

The magnetization M_z calculated using BMFT is displayed as a function of magnetic field in Fig. 4a for three sets of coupling values also used in Ref.². Because all the states are gapped in zero field, the magnetization remains zero for all fields smaller than the zero-field gap. This is clearly observed in Fig. 4a. Our curves for M_z compare very well qualitatively with existing numerical results^{2,3}. For certain coupling values a plateau appears at $M_z = 0.25$ which means that on average half the spins are aligned along the magnetic field. Remember that $M_z = 0.5$ is the saturation value. The frustration stabilizes this state, and as J_\times increases the size of the plateau also increases. The $(J/J_\perp, J_\times/J_\perp)$ and (α_1, α_2) phase diagrams in Figs. 4b and 4c show the region where the plateau at $M_z = 0.25$ appears. Here, $\alpha_1 = J_\perp/J$ and $\alpha_2 = J_\times/J$. This plateau region is larger than, and encompasses, the numerically calculated plateau region². We find that the plateau appears as J_\times increases only when $J_\perp \geq 0.67J$. Also, when $J_\times \gg J_\perp$ the plateau disappears. The sharp boundaries in the $M_z = 0.25$ phase diagrams only appear at $T = 0$. At finite temperature they are replaced by crossovers. Note that the $(J/J_\perp, J_\times/J_\perp)$ phase diagram is symmetric with respect to the diagonal because the Hamiltonian is symmetric under exchanging the J and J_\times terms¹.

The effect of temperature on the magnetization, and on the magnetization plateau is illustrated in Fig. 6a. As temperature increases the size of the plateau decreases, and eventually disappears altogether at high enough temperature. Because of thermal excitations, spins originally locked in the gapped state at zero temperature become available for alignment along the magnetic field. This leads to the linear increase of magnetization in the low-field regime for $T = 0.3J_\perp/k_B$; Fig. 6a. At $T = 0$ there is a critical field at which the magnetization reaches the saturation value $M_s = 1/2$, but for nonzero temperatures the critical behaviour is replaced by a crossover regime in a way similar to what was found for the Heisenberg chain and two-leg ladder in the absence of frustration⁷.

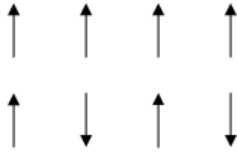


FIG. 5: An instantaneous configuration where on average the magnetization per site $M_z = 0.25$. For simplicity all the spins on one chain are ferromagnetically arranged while on the other chain they are antiferromagnetically arranged.

C. Spin bond parameters

The bond-mean-field parameters are shown in Figs. 6b and 6c for $J = 0.5J_\perp$ and $J_\times = 0.4J_\perp$. At the plateau, statistically half of the spins have been aligned with the magnetic field because $M_z = 0.25$. Surprisingly, the bond-mean-field parameters also adopt half of their maximum value. The maximum value of Q and P' is their value when $J_\perp = h = 0$. The maximum value of P is 0.5. For simplicity imagine an instantaneous configuration where all the spins on one chain align along one direction, whereas the spin on the other chain which are antiferromagnetically arranged. This is illustrated in Fig. 5. In this case, the average magnetization per site is $M_z = 0.25$, and exactly half of the rung bonds, one of the chains, and half of the diagonal bonds are antiferromagnetically arranged. The bond parameters represent the average AF correlations in the directions along which they are calculated, so each of them adopts half of its maximum value in zero field. The bond parameters vanish in the strong field regime, where the state labeling becomes obsolete and all three free energies equal. The bond parameters vanish at the same field where the magnetization reaches saturation signaling in this way a quantum (zero- T) phase transition⁷.

When $T > 0$, thermal fluctuations spoil this transition. A crossover behaviour replaces the zero- T critical behaviour exactly in the same way as in the Heisenberg chain and non-frustrated two-leg ladder⁷. At high enough temperature the plateaus in the bond parameters disappear; Figs. 6b and 6c.

D. Uniform spin susceptibility

For convenience, in this section the unit of energy is J rather than J_\perp . The magnetic susceptibility $\chi = \frac{\partial M_z}{\partial h}$ is shown as a function of field for three different couplings in Fig. 7a at temperature $k_B T/J = 0.01J$, and for three different temperatures in Fig. 7b for $\alpha_1 = J_\perp/J = 1$ and $\alpha_2 = J_\times/J = 0.5$. For $\alpha_1 = 1$ and $\alpha_2 = 0$, χ is characterized by two peaks only, and is zero for low fields because of the energy gap. As α_2 increases χ shows more structure and a gap. The gap in χ is due to the plateau at $M_z = 0.25$. Thermal fluctuations round-off the peaks and close the gaps in χ in agreement with the disappearance of the plateau at high enough temperatures.

E. Interpretation of the results

The magnetization plateau and its behaviour in general can be explained using the chemical potential and energy band filling of the JW fermions in the same way as in Ref.⁷. The excitation energies E_{N1} and E_{N2} are plotted in figure 8a as functions of wavenumber k for two different values of field h , and for $J = 0.5J_\perp$ and $J_\times = 0.4J_\perp$. When $h = 0$, the chemical potential of the JW fermions is zero; so only the lower-energy bands E_{N3} and E_{N4} are filled. A glance at Eq. (12) reveals that since two out of four bands are filled it is clear that $M_z = 0$. As the field increases, the chemical potential of the JW fermions increases. For fields h smaller than the energy gap, M_z remains zero. For the present set of exchange coupling constants, h must be greater than $0.57J_\perp$, which is the value of the energy gap in the absence of a magnetic field, in order to get a nonzero magnetization;

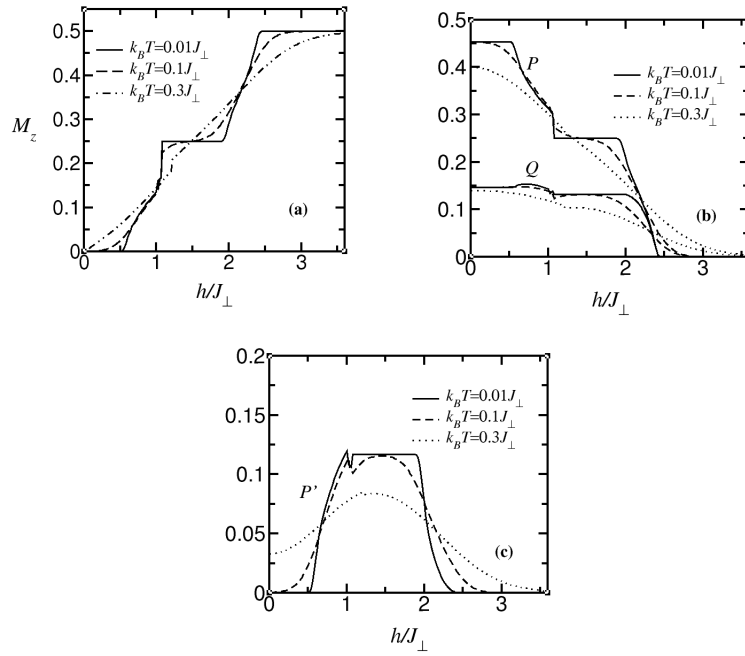


FIG. 6: The magnetization in (a) and the spin bond parameters in (b) and (c) are plotted as functions of magnetic field for three different temperatures; $k_B T = 0.01J_\perp$, $k_B T = 0.1J_\perp$ and $k_B T = 0.3J_\perp$. The exchange coupling constants are $J = 0.5J_\perp$ and $J_\times = 0.4J_\perp$.

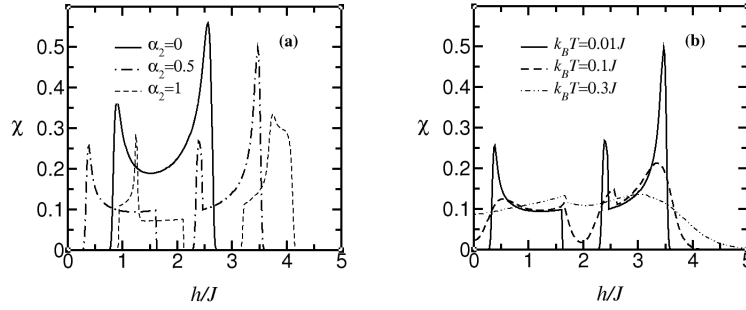


FIG. 7: The susceptibility $\chi = \frac{\partial M_z}{\partial h}$ is plotted as a function of h/J for (a) three coupling values at $k_B T/J = 0.01$, and (b) three temperatures with $\alpha_1 = 1$ and $\alpha_2 = 0.5$.

i.e., for fields greater than this threshold value the population of the higher-energy bands increases as field increases, leading to an increasing magnetization M_z . At $h = 1.1J_\perp$ the state of the system becomes the R-type state. The excitation energies E_{R1} and E_{R2} are plotted in Fig. 8b as functions of k for two different values of field. The energy bands in the R-type state are separated by a gap for certain coupling values whereas in the other two states they are not. From $h = 1.1J_\perp$ to $h = 1.9J_\perp$ three of the bands are populated and the fourth is empty so that there is a plateau at $M_z = 0.25$. Further increasing the field increases the population of the fourth band until it becomes completely full at $h = 2.42J_\perp$. At this point $M_z = 0.5$, and further increasing the field can no longer increase the population of the JW fermions. This results in the saturation of the magnetization M_z .

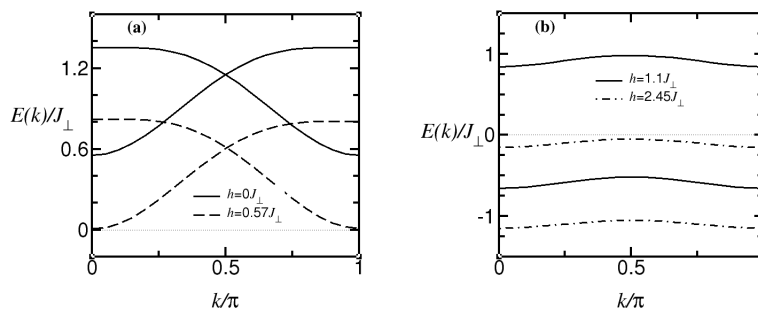


FIG. 8: (a) The energies E_{N1} and E_{N2} are plotted as functions of wavenumber k for $h = 0J_{\perp}$ and $h = 0.5J_{\perp}$. (b) The energies E_{R1} and E_{R2} are plotted as functions of k for $h = 1.1J_{\perp}$ and $h = 2.45J_{\perp}$. Here, $J = 0.5J_{\perp}$, and $J_{\times} = 0.4J_{\perp}$.

IV. CONCLUSION

In this work we analyzed the interplay between the quantum criticalities induced by frustration and magnetic field in the two-leg antiferromagnetic Heisenberg ladder. When frustration is introduced in the presence of a magnetic field a plateau appears at half the saturation magnetization. The plateau in the magnetization appears because of the onset of an energy gap between two (excitation) energy bands. As frustration increases this plateau increases in size indicating that this phase is stabilized by the frustration. Our results agree qualitatively well with existing numerical data of Sakai and Okazaki. In the presence of frustration, the system is characterized by three spin bond parameters, one along the chains, one along the rungs and one along the diagonals. These parameters vanish in the strong field limit signaling the occurrence of a zero- T phase transition. The latter give place to a crossover behaviour when temperature becomes nonzero. The magnetization plateau shrinks as temperature increases, and disappears in the high- T regime. The spin-bond parameters are also characterized by a plateau that disappears in the high- T regime.

Acknowledgments

We wish to acknowledge the financial support of the Natural Science and Engineering Research Council of Canada (NSERC), and of the Laurentian University Research Fund (LURF).

* Electronic Address: mazzouz@laurentian.ca

¹ B. Ramakko and M. Azzouz, Phys. Rev. B **76**, 064419 (2007).

² T. Sakai and N. Okazaki, Journal of Applied Physics **87**, 5893 (2000).

³ A. Honecker, F. Mila, and M. Troyer, Eur. Phys. J. B **15**, 227 (2000).

⁴ M. Azzouz, Phys. Rev. B **48**, 6136 (1993).

⁵ B. Bock and M. Azzouz, Phys. Rev. B **64**, 054410 (2001).

⁶ M. Azzouz, L. Chen, and S. Moukouri, Phys. Rev. B **50**, 6233 (1994).

⁷ M. Azzouz, Phys. Rev. B **74**, 174422 (2006).

⁸ N.D. Mermin and H. Wagner, Phys. Rev. Lett. **17**, 1133 (1966).

⁹ P. Jordan and E. Wigner, Z. Phys. **47**, 631 (1928).

¹⁰ I. Affleck and J.B. Marston, Phys. Rev. B **37**, 3774 (1988).

¹¹ J. des Cloiseaux and J.J. Pearson, Phys. Rev. **128**, 2131 (1962).